Korean J. Chem. Eng., 39(10), 2636-2651 (2022)
DOI: 10.1007/s11814-022-1178-0

pISSN: 0256-1115
eISSN: 1975-7220

Investigating the effect of different nanoparticles on thermo-economic optimization of gasket plate heat exchanger

Mohammad Shafiey Dehaj, Hassan Hajabdollahi†, and Mohammad Ataeizadeh

Department of Mechanical Engineering, Vali-e-Asr University of Rafsanjan, Rafsanjan, Iran
(*Received 15 January 2022 • Revised 13 April 2022 • Accepted 14 May 2022*)

Abstract−This paper reports an investigation into the effects of different nanoparticles, including copper oxide, zirconium oxide, aluminum oxide, and silicon oxide nanoparticles, on thermoeconomic optimization of the gasket plate heat exchanger (GPHE). Effectiveness and total annual cost (TAC) were selected as two objective functions simultaneously. The non-dominated sorting genetic algorithm (NSGA-II) with seven design variables involving particle volumetric concentration and geometrical parameters of the GPHE was used for optimization. Results showed that TAC versus effectiveness was improved when nanoparticles were applied. The results of the optimization show that heat exchanger thermoeconomic parameters are better improved in the case of copper oxide as nanoparticles and generally followed by zirconium oxide, aluminiom oxide, silicon oxide. For example, 2.61% growth in the effectiveness and 6.8% reduction in the TAC are observed in the case of copper oxide nanoparticles compared with the case of without nanoparticles. The effectiveness and TAC decreased with an increase in the corrugation wavelength, while an enhancing in the plate length of the GPHE leads to an increase in effectiveness and TAC. Also, the results indicate that with an enhancement of the particle volumetric concentration of nanoparticles, effectiveness and TAC were increased linearly. Finally, the effect of the price of different nanoparticles on TAC was studied.

Keywords: Nanofluid, Gasket Plate Heat Exchanger, NSGA-II, Objective Function, Particle Volumetric Concentration

INTRODUCTION

Irrespective of their models and their working fluids, heat exchangers include shell and tube heat exchangers, multi-tube heat exchangers, and GPHEs and provide heat transfer in two or more fluids with various temperatures. GPHEs are applied in power generation plants, food industries, and petroleum and oil industries. Global warming, climate change, greenhouse gas emissions, the high cost of energy, and energy wastes are serious issues around the world, which have motivated people and scientists to improve energy systems. Due to the extensive application of heat exchangers and energy crisis in the world and the importance of effectiveness enhancement in energy systems, it is important to improve heat exchanger effectiveness.

The use of turbulent instruments in the flow path is a way to improve the total coefficient of heat transfer and effectiveness [1,2]. There are many studies available on the design and optimization of heat exchangers. Thermal and hydraulic optimization of water to water chevron type plate heat exchanger was presented by Imran et al. [3]. They found that pressure drop and heat transfer increase with increase in number of thermal plates and horizontal port center distance. Cagin et al. [4] studied the performance of GPHE with three different plates and showed that thermal and hydraulic properties reduce with decreasing the plate's coordination. Abdullah et al. [5] numerically and experimentally investigated a chevron-type heat exchanger and found that the numerical results and experimental date were in suitbale agreement. Shokouhmand et al. [6] studied the effect of flow maldistribution on the optimal design of a plate heat exchanger using constrained multi objective genetic algorithm. Thermal behavior of the flow boiling of a complex nanofluid in a rectangular channel was explored by Hayder et al. [7]. Yongfeng et al. [8] evaluated multiple semi-twisted tape inserts in a heat exchanger pipe using Al_2O_3 nanofluid. Gholap et al. [9] designed and optimized a heat exchanger using multi-objective optimization to minimize energy and consuming cost. Improvement of heat transfer and critical heat flux (CHF) via nanofluid in pool boiling was examined by Hayder et al. [10]. Multiphase flow and boiling heat transfer modelling of nanofluids in horizontal tubes embedded in a metal foam was investigated by Hayder et al. [11]. They found that by decreasing the porosity and increasing the pore density of the metal foam, higher volume fraction of vapor and pressure drop are achieved in the pipe outlet. Hajabdollahi et al. [12] designed GPHE with an optimum design using a multimodal genetic algorithm. They found that the chevron corrugation wavelength parameter, plate width, and plate surface area (length *width) had an important impact on the contrast between the objective functions. In addition to the mentioned methods, pressure drop and cost increase (the cost of using additional equipment and pressure drop increase) further increase the effectiveness.

Although different methods have been used to enhance the effectiveness of heat exchangers, the application of nanoparticles with better heat properties than base fluids, e.g., water and ethyl glycols, has generated interest in the use of solid particles in base fluids. For instance, thermal conductivity is one of these properties with a

†To whom correspondence should be addressed.
E-mail: h.hajabdollahi@vru.ac.ir
Copyright by The Korean Institute of Chemical Engineers.

direct influence on the coefficient of heat transfer. It is good to mention that solid particles in milli and micro sizes deposit faster and occlude the flow path, causing erosion in pipelines and further pressure drop in pipes, while nanofluids compared to the current methods for heat transfer enhancement have a great potential for increasing the heat transfer rate in heating systems, which would decrease the pressure drop in the flow path.

Hayder et al. [13] performed an experimental investigation of nanoparticle concentration, boiler temperature and flow rate on flow boiling of zinc bromide and acetone solution in a rectangular duct. They found that the stability of the acetone/$ZnBr_2$ based Graphene is mainly dependent on the density of the base fluid ($ZnBr_2$ concentration). Vajjha et al. [14] studied the thermal conductivity of three various nanofluids and provided a new correlation that covers the vast majority of nanoparticle concentrations and temperatures experimentally. They found it useful to use nanofluids in high-temperature environments because of the improvement in thermal conductivity at higher temperatures. The effects of temperature and nanofluid volumetric concentration on thermophysical properties, heat transfer effectiveness, and pumping power were addressed by Vajjha et al. [15]. Sharma et al. [16] used past research, datasets of previous studies, and nonlinear regression to provide some single relationships for thermophysical properties of nanofluid flows (thermal conductivity and viscosity) as well as coefficient of heat transfer and friction factor so that it can be employed for a significant number of nanoparticles accurately enough. Lotfi et al. [17] investigated the convective heat transfer coefficient of various nanofluids and compared various approaches numerically.

Extensive studies and investigations are being conducted on heat exchangers and the use of nanofluids in heat exchangers. Some researchers have experimentally investigated employing nanofluids in heat exchangers and many have used numerical methods to design and optimize heat exchangers with one and multi-objective optimization methods. Thierry et al. [18] studied the heat effectiveness of plate heat exchangers at low temperatures by using two nanofluids. They found that in laminar flow, the coefficient of convective heat transfer for aluminum oxide and CNTs was enhanced by 42% and 50%, respectively, compared to distilled water at the same Reynolds number. Guo [19] reviewed and summarized the application of nanofluids to increase heat transfer, a variation of experimental measurement and numerical models of thermophysical and thermal properties of nanofluids and improvement mechanisms revealed. Fluid performance in a plate heat exchanger with different nanofluids was studied by Arun Kumar et al. [20]. Pantzali et al. [21] investigated nanofluid operation as a cooling fluid in plate heat exchangers. Vikas Kumar et al. [22] looked at the effect of a chevron angel (60 and 30 degrees) on the thermal performance of plate heat exchangers with ZnO/water nanofluid that had 0.5-2% volumetric concentration. They found that when the volumetric concentration of nanoparticles was 1%, parameter performance was in the best responses. Taghizadeh et al. [23] investigated the TiO_2/water nanofluid usage in a plate heat exchanger of milk pasteurized industries. They evaluated negative and positive aspects of the nanofluid application in plate heat exchangers and the effectiveness prominent parameter was introduced. Their results established the possible use of this nanofluid in plate heat exchangers. Dan et al. [24] investigated the pressure drop and convection heat transfer coefficient of different nanofluids in chevron heat exchangers. Hajabdollahi et al. [25-27] examined the effects of shapes of nanoparticles on the thermoeconomic optimization of a gasket plate heat exchanger, tubular heat exchanger network and fin and tube heat eaxchanger filled by boehmite alumina nanofluid. They indicated that the nanofluids involving cylinder, blade and brick shaped nanoparticles have the best performance, respectively.

The key purpose of present study was to investigate the influence of different nanoparticles on thermo-economic optimization of a gasket plate heat exchanger, and the results were compared with each other and with the case without nanoparticles. Due to the application of GPHE in various industries, the present results could be found useful.

As a summary, the following are the contribution of this study into the subject:

- Thermoeconomic modeling and multi-objective optimization of the GPHE in the presence of different nanoparticles.
- Optimization was done with a fast and elitist non-dominated sorting genetic (NSGA-II) algorithm by seven decision variables, including the volumetric concentration of nanoparticles, amplitude and wavelength of corrugation, width and length of plate, corrugation angle, and the number of plates in different cold mass flow rates.
- Copper oxide (CuO), zirconium oxide (ZrO_2), aluminum oxide (Al_2O_3) and silicon oxide (SiO_2) nanoparticles were used at different volumetric concentrations ranging from 0% to 4% in base fluid (water) as a cooling fluid on thermoeconomic improvement of GPHE parameters and comparing the results with different of nanoparticles and with the case of base fluid (without nanoparticle).

THERMAL MODELING

A schematic diagram of the GPHE is in Fig. 1. Since two inlet temperatures were known, effectiveness-number of transfer unit or ε-NTU procedure was used in this research. In this well-known method, the effectiveness for each type of heat exchanger is available in terms of NTU, ratio of heat capacity (C^*) as well as stream direction [1]. In fact, by having NTU and C^*, effectiveness could be determined, which is discussed as below.

Effectiveness for the counterflow heat exchanger is obtained as [1]:

$$\varepsilon = \frac{1-e^{-NTU(1-C^*)}}{1-C^* e^{-NTU(1-C^*)}} \tag{1}$$

where C^* and NTU are described as [12]:

$$C^* = \frac{C_{min}}{C_{max}} \tag{2}$$

$$NTU = \frac{UA_{tot}}{C_{min}} \tag{3}$$

$$C_{min} = \min((\dot{m}c_p)_c \cdot (\dot{m}c_p)_h) \tag{4}$$

$$C_{max} = \max((\dot{m}c_p)_c \cdot (\dot{m}c_p)_h) \tag{5}$$

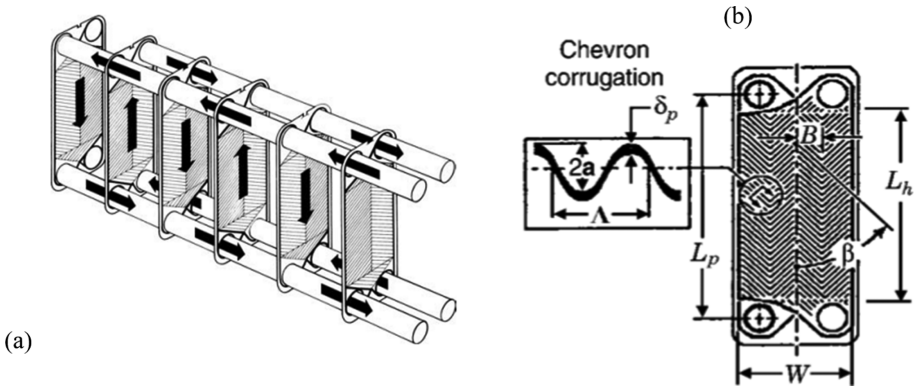


Fig. 1. Schematic of GPHE with chevron corrugated plate.

In the above equations, $\dot{m}$ is mass flow rate and subscripts h and c refer to the hot and cold side streams, respectively. Furthermore, the total coefficient of heat transfer (U) and total heat transfer surface area (A_{tot}) was calculated from following equations [12]:

$$U=\frac{1}{\frac{1}{h_c}+R_{f,h}+\frac{t}{k_p}+R_{f,c}+\frac{1}{h_h}} \tag{6}$$

$$A_{tot}=2\times\phi\times W\times L_p\times N_p \tag{7}$$

$$\phi=\frac{1}{6}(1+\sqrt{1+X^2}+4\sqrt{1+0.5X^2}) \tag{8}$$

where W, L_p, N_p, ϕ,t. $R_{f,c}$ and R_{fh} are plate width, plate length, number of plates, dimensionless number, plate thickness, and cold- and hot-side fouling resistance factor, respectively. Furthermore, h_c and h_h are cold- and hot-side coefficients of convective heat transfer, respectively, which are provided in the below sub-sections.

1. Heat Transfer Coefficient and Friction Factor on the Cold Side

Several various mathematical relations for the heat transfer and pressure drop in chevron plate (Fig. 1) heat exchangers have been presented in the texts. The formulation of the cold-side Fanning factor (f) and Nusselt number (Nu) is estimated as below [28]:

$$f=\frac{k_1}{Re^{k_2}} \tag{9}$$

$$Nu=\frac{hD_h}{k}=0.205Pr^{\frac{1}{3}}\left(\frac{\mu_m}{\mu_w}\right)^{\frac{1}{6}}(f.\,Re^2\sin 2\beta)^{0.374} \tag{10}$$

in which β is the angle of corrugation. The above correlations are valid for β in the range of 10-80° within ±13 deviation. Note that the values of μ_m and μ_w should be calculated from the average temperature of the stream and the temperature of wall, respectively. Furthermore, values of k_1 and k_2 are given in [28] as functions of Reynolds number for various values of chevron angles.

In addition, Prandtl number (Pr) and (Re) Reynolds number are related to the mass flux, hydraulic diameter, and viscosity evaluated as [1]:

$$Pr=\frac{\mu c_p}{k} \tag{11}$$

$$Re=\frac{GD_h}{\mu} \tag{12}$$

$$D_h=\frac{4a}{\phi} \tag{13}$$

$$X=\frac{2\pi a}{\Lambda} \tag{14}$$

in which G is the mass flux calculated as [12]:

$$G=\frac{\dot{m}}{2aW} \tag{15}$$

where a and Λ are the amplitude and wavelength of chevron corrugations, respectively. Finally, the total pressure drop is estimated as below [28]:

$$\Delta P=2\rho fG^2\frac{L_pN_p}{D_h}\left(\frac{\mu_m}{\mu_w}\right)^{-0.17} \tag{16}$$

where N_p is the number of plates and L_p is the total length of plate as illustrated in Fig. 1.

2. Base Flow and Nanoparticle Properties

In this study, water is considered as the base flow and its properties, such as thermal conductivity, heat capacity and density, are evaluated at the average temperature of inlet and outlet. In fact, the mentioned properties are available in terms of temperature and developed code selected them by interpolation method.

Different nanoparticles, including copper oxide (CuO), zirconium oxide (ZrO_2), aluminum oxide (Al_2O_3), and silicon oxide (SiO_2), were used with water to prepare the nanofluid on the cold side to enhance the heat transfer rate. In addition to the wide availability of the mentioned nanoparticles, thermo-physical properties for these types of nanoparticles are developed well, which this is the main reason for selection of these particles. Furthermore, the thermal conductivity for these type of nanoparticles is high which leads to the higher rate of heat transfer and effectiveness.

Thermophysical properties of nanofluid flows including density (ρ), thermal conductivity (k), specific heat (c_p), and dynamic viscosity (μ) were estimated as below [16]:

$$\rho_{NF}=(1-\emptyset)\rho_{BF}+\emptyset\rho_{NP} \tag{17}$$

$$c_{P,\,NF}=\frac{(1-\emptyset)(\rho c_p)_{BF}+\emptyset(\rho c_p)_{NP}}{(1-\emptyset)\rho_{BF}+\emptyset\rho_{NF}} \tag{18}$$

$$\frac{\mu_{NF}}{\mu_{BF}} = C_1(1+\emptyset)^{11.3}\left(1+\frac{T_{NF}-273.15}{70}\right)^{-0.038}\left(1+\frac{d_{NP}}{170}\right)^{-0.061} \quad (19)$$

$$\frac{k_{NF}}{k_{BF}} = 0.8938(1+\emptyset)^{1.37}\left(1+\frac{T_{NF}-273.15}{70}\right)^{0.2777}\left(1+\frac{d_{NP}}{150}\right)^{-0.0336}\left(\frac{\alpha_{NP}}{\alpha_{BF}}\right)^{0.01737} \quad (20)$$

where Ø, T, d, C_1 and α are the particle volumetric concentration (PVC), nanoparticle temperature, diameter, type constant of nanoparticle, and thermal diffusivity factor, respectively. Also, the subscripts NP, BF and NF indicate nanoparticles, base fluid, and nanofluid, respectively. Equations 19 and 20 are valid for the base fluid of water, $293.15<T_{NF}<340.15$, $20<d_{NP}<100$ and $0\le\emptyset\le0.04$ with a maximum error of ±%10.

OPTIMIZATION

Adding nanoparticles in the base fluid will enhance both the heat transfer and friction factor. Accordingly, heat transfer improves the result in pressure drop is enhanced. Consequently, there is a conflict between the heat transfer rate and pressure drop in the applying of nanofluid instead of base fluid as working fluid. Optimization was done with the fast and elitist NSGA-II algorithm by seven decision variables and two objective functions.

1. Objective Functions, Design Parameters

For evaluating both influences, effectiveness and TAC (including investment cost and operating cost) were chosen as objective functions in the present research. Effectiveness is described in Eq. (1) and TAC is expected as below [12]:

$$TAC(\$/year)=a_f C_{in}+C_{op} \quad (21)$$

$$C_{in}(\$)=C_A\times A_{tot}^{n}+C_{NP} \quad (22)$$

$$a_f=\frac{i}{1-(1+i)^{-y}} \quad (23)$$

where a_f, C_{in}, i, and y are annualized factor, cost of investment, interest rate, and depreciation time, respectively. C_A and n are constants, and C_{NP} denotes the cost of nanoparticles provision computed as follows:

$$C_{NP}=m_{NP}*Z_{NP} \quad (24)$$

where m_{NP} and Z_{NP} are the needed mass and the unit price of nanoparticles, respectively. The operational cost related to the pumping power of both hot and cold flow is calculated as follows [12]:

$$C_{op}=\left(\frac{\$}{year}\right)=\left(\left(k_{el}\tau\frac{\Delta PV_t}{\eta}\right)_c+\left(k_{el}\tau\frac{\Delta PV_t}{\eta}\right)_h\right) \quad (25)$$

where η, τ and k_{el} are pump effectiveness, hours of operation, and unit price of electricity, respectively.

Decision variables include the volumetric concentration of nanoparticles, amplitude and wavelength of corrugation, width and length of plate, corrugation angle, and the number of plates in different cold mass flow rates.

2. Case Study

In the present investigation, various nanoparticles, such as CuO, ZrO_2, Al_2O_3 and SiO_2, with an average diameter of 29 nm were selected and used in a gasket plate heat exchanger. The input model data presented in Table 1 were selected for modeling. Oil with inlet temperature of 70 °C and with a mass flow rate 3 kg/s was chosen as the hot stream which was cooled by water with an inlet temperature of 20 °C. Additionally, Table 2 shows the the properties of the nanoparticles used in this research. Lastly, to evaluate the results, optimization was carried out for various cold-side mass flow rates involving 1, 1.5, and 2 kg/s. The unit prices of CuO, ZrO_2, Al_2O_3 and SiO_2 are 250, 300, and 400 $/kg according to the existing market price. Genetic algorithm optimization was done for 1,000 generations, by a search population size of M=100 individuals, crossover probability of pc=0.9, gene mutation probability of pm=0.035, and controlled elitism value c=0.55. Fig. 2 illustrates the Pareto optimal curve, which noticeably indicates the conflict between the two objectives, i.e., the effectiveness and TAC. For developing the thermoeconomic modeling of GPHE, a confirmed code, which was extended by Hajabdollahi et al. [12], was applied.

Table 1. Constants considered as input parameters in the optimization

Parameter	Value
Mass flow rate of cold flow (kg/s)	1-1.5-2
Mass flow rate of hot flow (kg/s)	3
Inlet hot temperature (°C)	20
Inlet cold temperature (°C)	70
Fouling factor (cold stream) (m^2 W/K)	0.000086
Fouling factor (hot stream) (m^2 W/K)	0.00086
Insert rate (-)	0.1
Equipment life period (year)	10
Hours of operation per year (h/year)	5000
Price of electrical energy ($/MWh)	60
Pump effectiveness (-)	0.6

Table 2. Nanoparticle properties used in this study [16]

Nanoparticles	Thermal conductivity (W/m^2 K)	Density (kg/m^3)	Specific heat (J/kg K)
Al_2O_3	36	3,880	773
CuO	69	6,350	535
ZrO_2	1.7	5,500	502
SiO_2	1.4	2,220	745

RESULTS AND DISCUSSION

The essential aim of present research was to investigate the influence of four nanoparticles, including CuO, ZrO_2, Al_2O_3, and SiO_2, on thermoeconomic optimization of GPHE. The variations of the seven considered design parameters are provided in Table 3. Optimum results of using various nanofluids and water as working fluid were evaluated.

Optimum Pareto fronts without and with different nanoparticles at various cold-side mass flow rates involving 1, 1.5, and 2 kg/s are shown in Fig. 2 (the price of nanoparticles is 300 $/kg). The results reveal that the algorithm was correctly convergent and the optimal Pareto front for both case generally dominated. In fact, it can be said that nanoparticles (CuO, ZrO_2, Al_2O_3, and SiO_2) had a

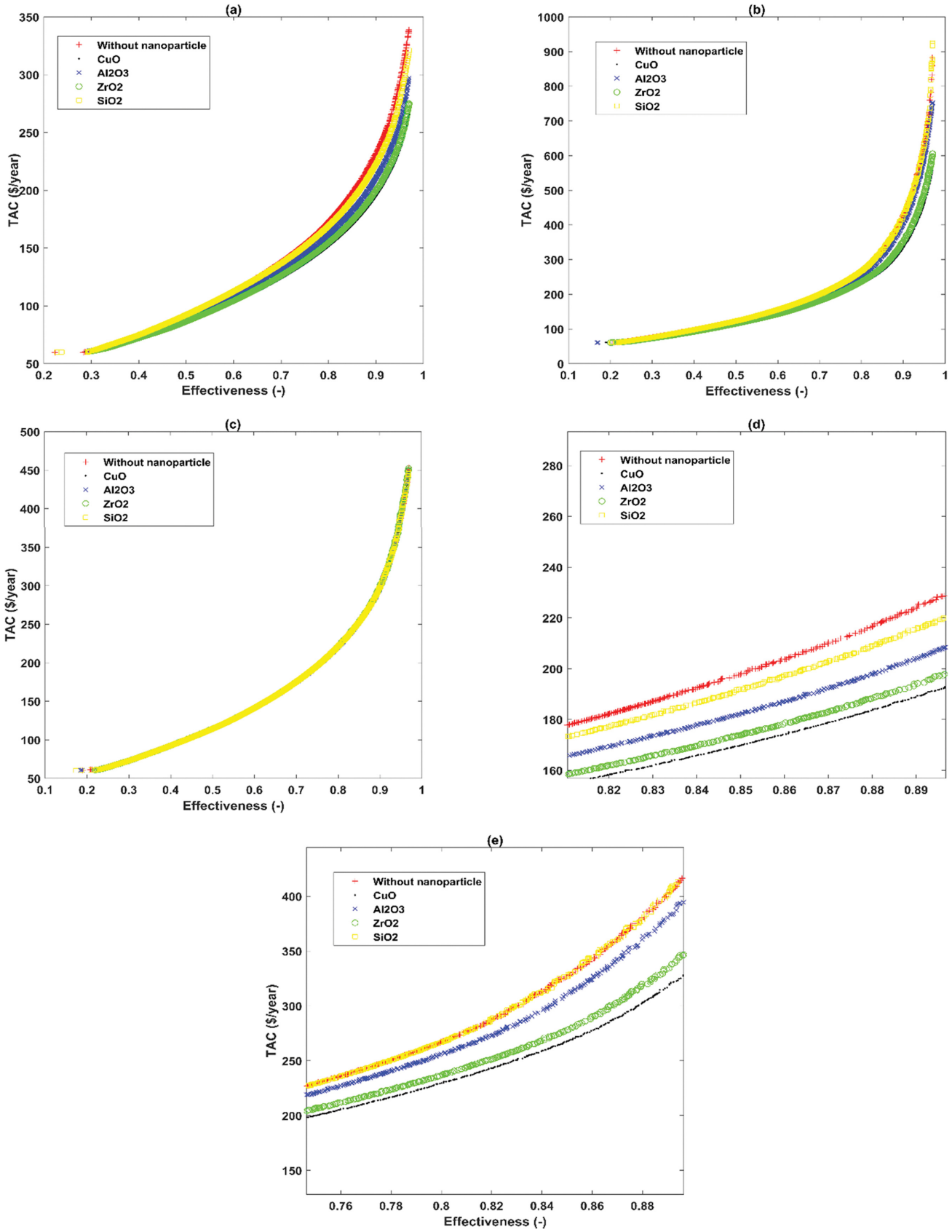


Fig. 2. Set of optimal solutions for fixed hot side mass flow rate of 3 kg/s and for different cold side mass flow rate in three cases studied (a): $\dot{m}_c$=1 kg/s, (b): $\dot{m}_c$=1.5 kg/s and (c): $\dot{m}_c$=2 kg/s, (d): Close-up view of Pareto fronts for the $\dot{m}_c$=1 kg/s, (e): Close-up view of Pareto fronts for the $\dot{m}_c$=1.5 kg/s.

Table 3. Decision variables and their range of variation

Decision variable	Lower bound	Upper bound
Corrugation angle (degree)	30°-45°-50°-60°-65°	
Corrugation wavelength (mm)	3	8
Corrugation amplitude (mm)	1	10
Plate width (m)	0.2	0.8
Plate length (m)	0.3	1
Number of plate (-)	10	100
PVC (-)	0	0.04

good significant effect at the lower cold-side mass flow rates of 1 and 1.5 kg/s, respectively. It can also be inferred that by adding the nanoparticles, the results of TAC versus effectiveness at the cold-side mass flow rate of 2 kg/s were almost the same as the results of the base fluid as depicted in Fig. 2(c). It can be said that at a high cold mass flow rate, the total coefficient of convective heat transfer is high enough and further improvement by nanoparticles does not result in a not noticeable enhancement in the total coefficient of heat transfer and hence the effectiveness of GPHE does not change significantly.

It can be found in Fig. 2(a) that the optimum results determine that GPHE thermo-economic parameters were improved to a greater extent when CuO was applied as the nanoparticle. It was generally followed by ZrO_2, Al_2O_3, and SiO_2.

In fact, the thermal conductivity of a fluid directly depends on the coefficient of heat transfer. The heat transfer coefficient is enhanced by the improvement of thermal conductivity. Since CuO nanoparticles have better thermal conductivity, it was quite predictable to make the greatest improvement.

In addition, by increasing the cold-side mass flow rate, the pressure drop on this side increased and the operational cost of the GPHE and consequently TAC increased as shown in Fig. 2.

To complete the optimization, the finest point had to be determined between the optimal points of the Pareto front. For this aim, the Linamp procedure was used [29]. In this procedure, after the objective functions are made dimensionless, the finest point is presented and the closest point to the finest point is designated as the final optimal solution [30]. The finishing values of the two objective functions (effectiveness and TAC) for the case without nanoparticles was used and the cases in which nanoparticles (CuO, ZrO_2, Al_2O_3, and SiO_2) were applied are presented in Table 4 for the Pareto front in Fig. 2(a). Also, the improvement of each objective function in the nanoparticle case was compared to the base fluid whose results are provided in Table 5. Actually, the effectiveness of the final optimum point in the state with CuO, ZrO_2, Al_2O_3, and SiO_2 nanofluids was significantly improved by 2.61%, 1.76%, 1.5%, and 0.56% relative to base fluid, respectively. In fact, the use of nanofluid improves the rate of heat transfer and consequently the effectiveness.

On the other hand, the final optimum values for the TAC of the case in which CuO, ZrO_2, and Al_2O_3 nanofluids were used were improved by 6.8%, 5.9%, and 2.59%, respectively. Although pressure drop increases in the presence of nanofluid for the fixed manufactured heat exchangers as compared with the base fluid, but the optimization algorithm could find an exchanger which has the lower pressure drop or operational cost. Actually, the optimization code finds the configuration (for example by decreasing the surface area or plate length) which leads to the lower pressure drop. As well, TAC was increased by 0.08% when SiO_2 nanoparticles were added.

Figs. 3-6 depict the effects of some design parameters on the effectiveness and TAC of the final optimum point for the states with nanoparticles (copper oxide, zirconium oxide, aluminum oxide, and silicon oxide) and without nanoparticles (base fluid). In these figures, the objective functions are plotted by changing the variables (specified within their upper and lower allowed limits). Fig. 3 shows the variations in TAC and effectiveness in terms of plane length variations for different nanofluids and the base fluid. By enhancing the plate length of the heat exchanger, the total area of the heat transfer was increased, and being constant the total coefficient of heat transfer increases the NTU by virtue of Eq. (3), and consequently, as is evident in Fig. 3, it increased the effectiveness. Moreover, according to Fig. 3, by enhancing the plate length, the amount of consumable material and the pressure drop were also increased and ultimately it increased the operating cost. Consequently, as shown in Fig. 3, TAC was increased.

Fig. 4 shows the variation in TAC and effectiveness in terms of corrugation wavelength variations for the cases with and without nanoparticles. According to Fig. 4, by enhancing the wavelength of corrugation, the effectiveness and TAC for the final optimum points were decreased. In fact, with increasing the corrugation wavelength, according to Eq. (8) and (14), the total area of the heat trans-

Table 4. Final optimum objective functions for the different cold side mass flow rates in three cases of without and with nanoparticles

	Without nanoparticle	CuO	ZrO_2	Al_2O_3	SiO_2
Effectiveness (-)	0.6462	0.6631	0.6576	0.6559	0.6498
TAC ($/year)	123.6	115.2	116.3	120.4	123.7

Table 5. Percent of improvement in effectiveness and TAC at $\dot{m}_c$=1 kg/s, $\dot{m}_h$=3 kg/s according to Fig. 2(a) in the case of "with nanoparticles" compared with the case of "without nanoparticles" (%)

Nanoparticles	CuO	ZrO_2	Al_2O_3	SiO_2
Percent of grown in effectiveness (%)	2.61	1.76	1.50	0.56
Percent of reduction in TAC (%)	6.8	5.9	2.59	−0.08

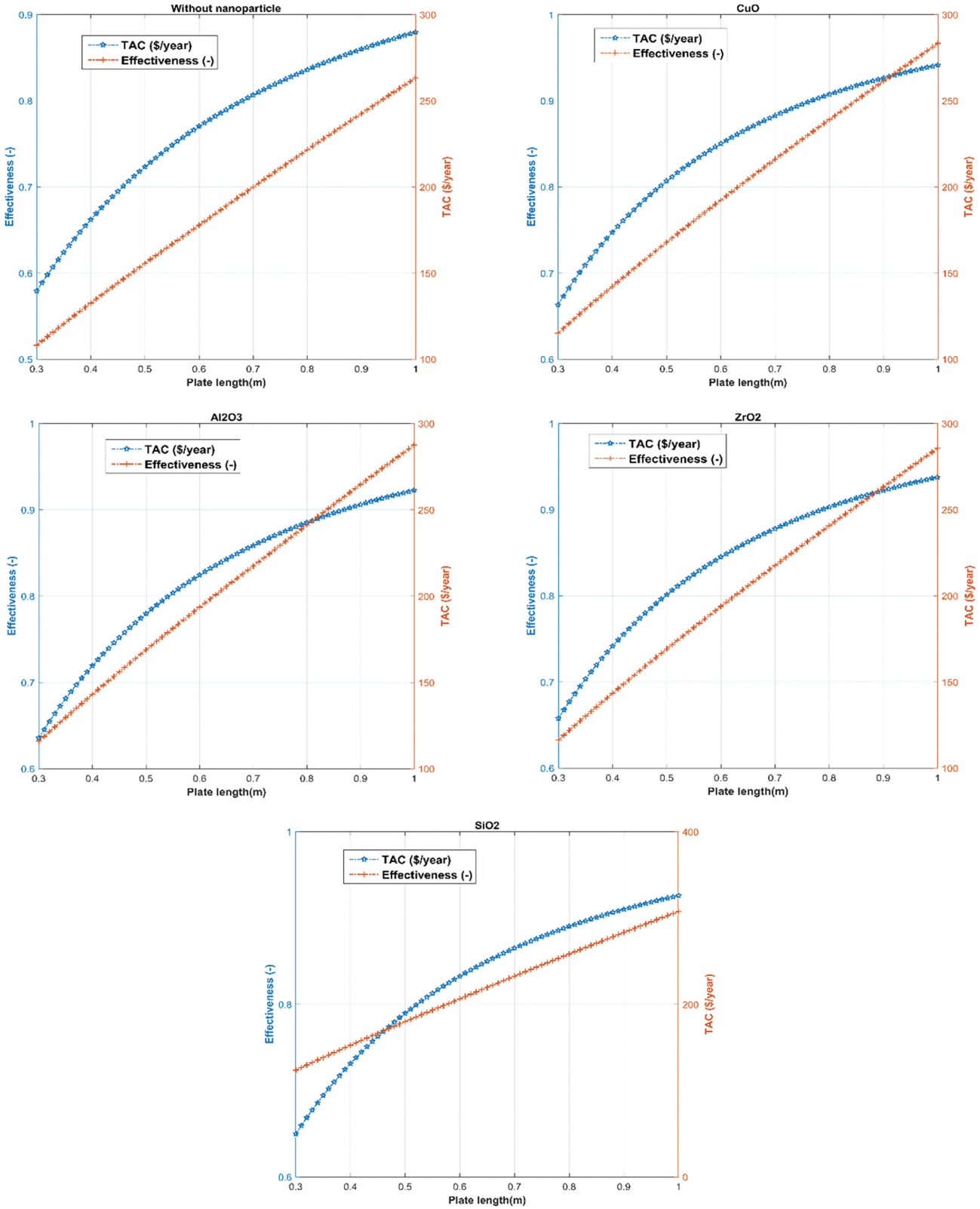


Fig. 3. Variation of objective functions (Total annual cost-Effectiveness) in terms plate length for different nanofluid and base fluid.

fer was reduced and, consequently, NTU was decreased according to Eq. (3), which, according to Fig. 4, reduced the effectiveness of the heat exchanger. In addition, reducing the friction factor and increasing the hydraulic diameter according to Eq. (16) resulted in decreasing the pressure drop, and accordingly the decrease the operational cost on the one hand and the reduction of the total area of

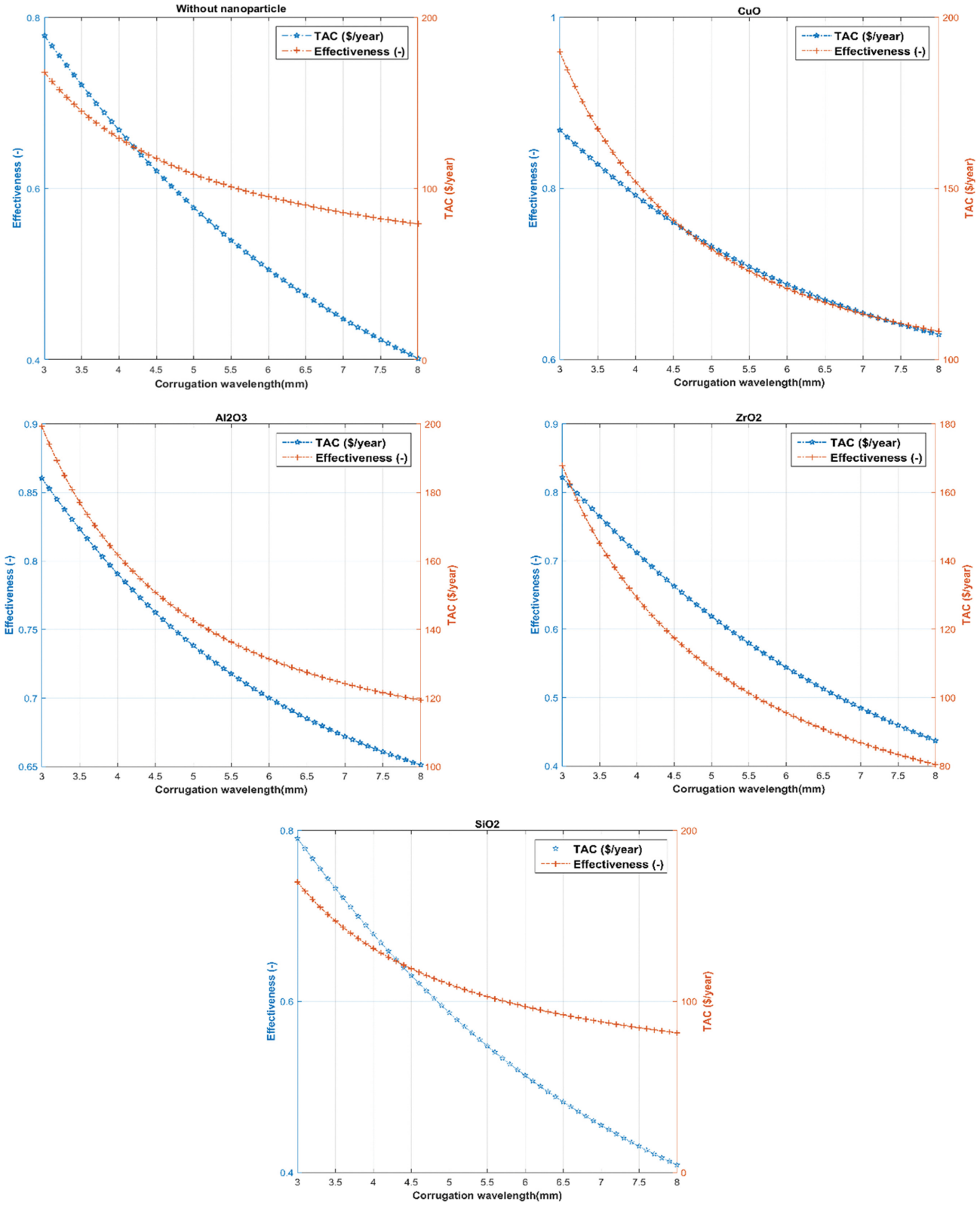


Fig. 4. Variation of objective functions (Total annual cost-Effectiveness) in terms corrugation wavelength for different nanofluid and base fluid.

heat transfer would reduce the investment cost. Finally, the reduction of investment costs and operating costs would reduce TAC as shown in Fig. 4.

Fig. 5 shows changes in TAC and effectiveness in terms of the number of plates for different nanoparticles and without nanoparticle (base fluid). As provided in Fig. 5, by enhancing the number

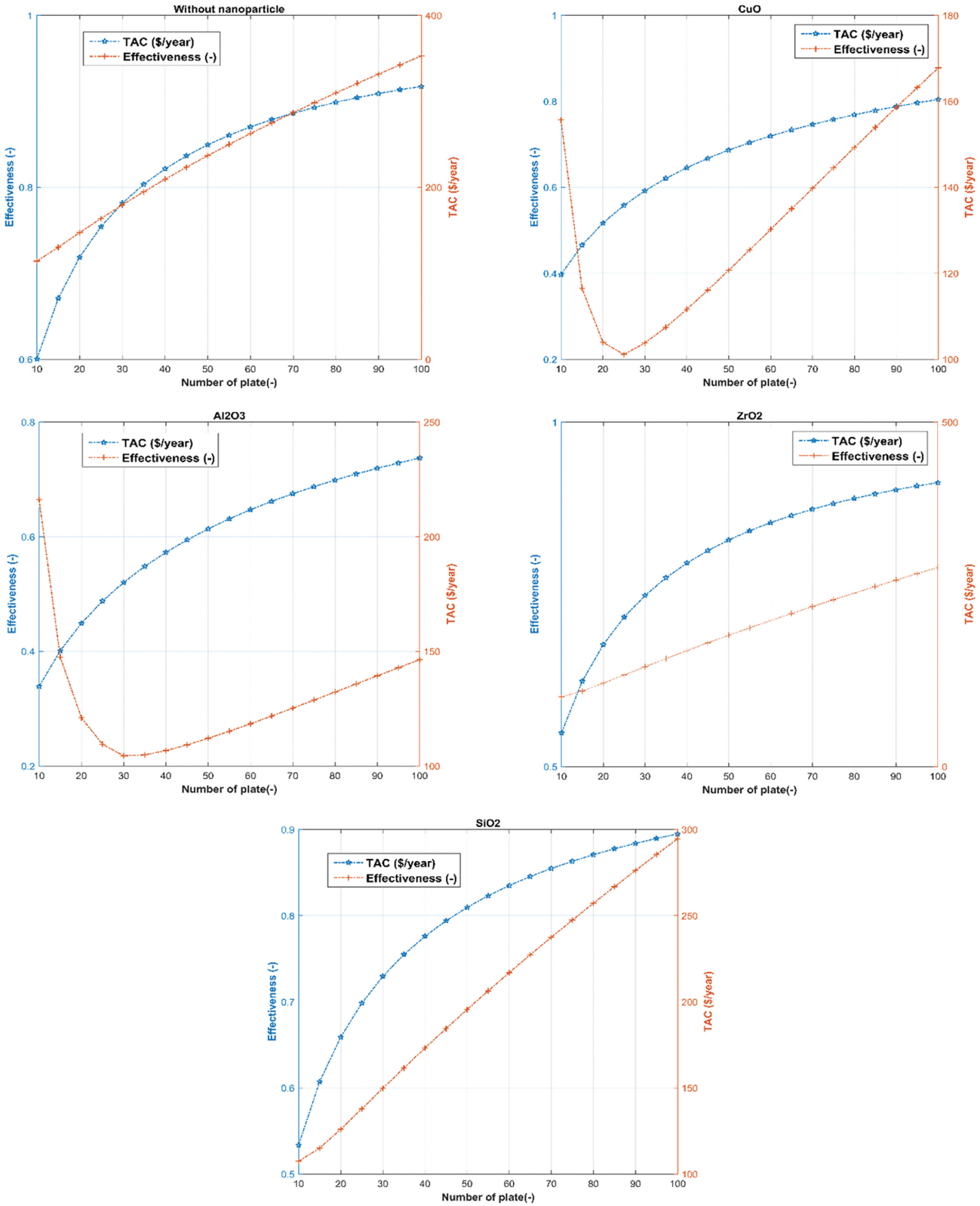


Fig. 5. Variation of objective functions (Total annual cost-Effectiveness) in terms of number of plates for different nanofluid and base fluid.

of plates, the effectiveness and TAC were increased. This is related to the fact that as the number of plates is improved, the total area of the heat transfer increases, which increases the NTU and ultimately increases the effectiveness of the heat exchanger. Thus, by increasing the number of plates, the pressure drop increased. In addition, by increasing the number of plates, the cost of the con-

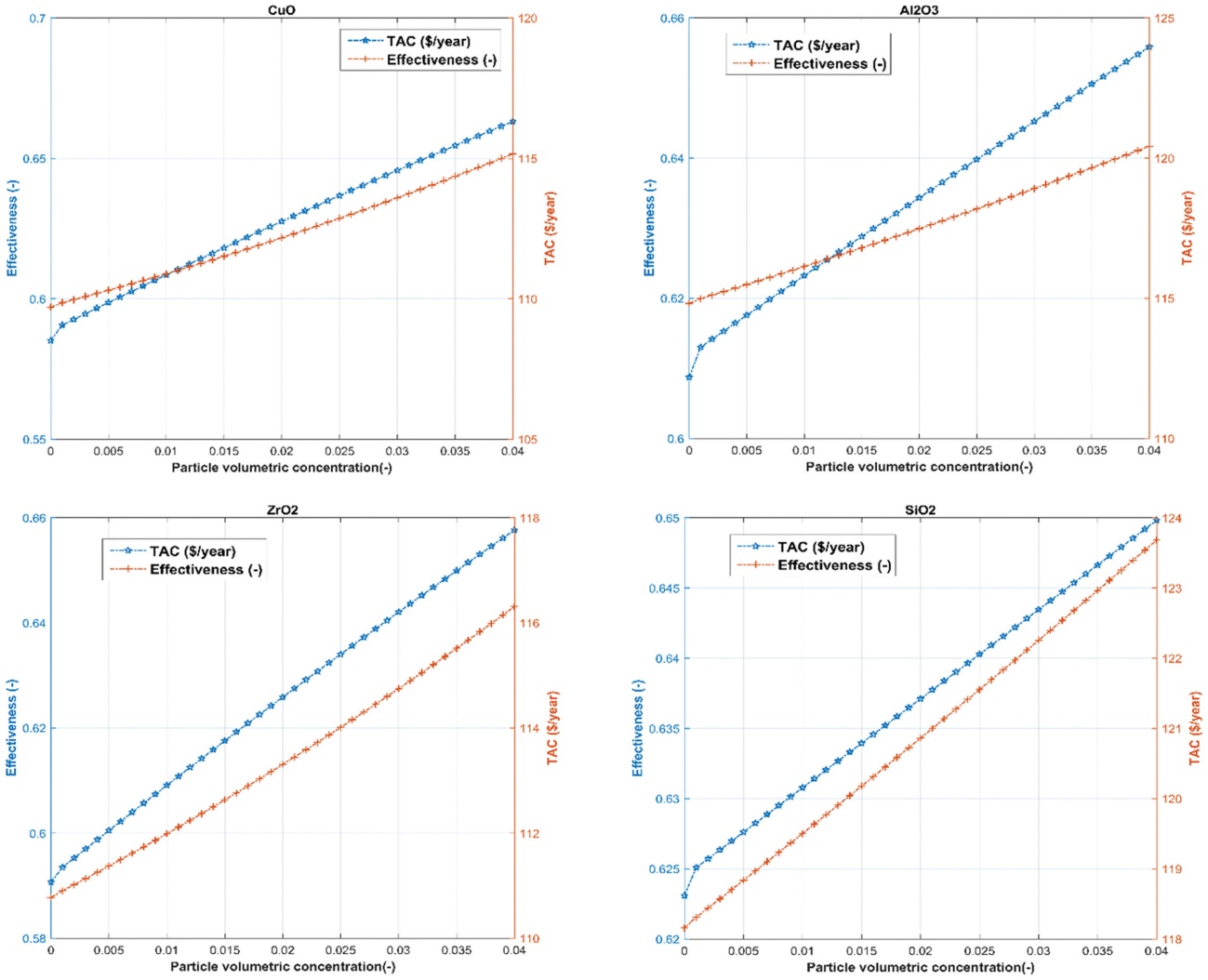


Fig. 6. Variation of objective functions (Total annual cost-Effectiveness) in terms of particle volumetric concentration for different nanofluid.

sumable material increased (which is considered in the investment cost). The same factors increased the operating cost and, consequently, TAC.

Fig. 6 shows variations in the objective functions in terms of the particle volumetric concentrations of nanoparticles for copper oxide, zirconium oxide, aluminum oxide, and silicon oxide nanofluids. As shown in Fig. 6, effectiveness and TAC were increased linearly. In fact, an enhancement of the nanofluid concentration leads to an improvement of effectiveness. Since the thermal conductivity of the fluid is depending on the coefficient of heat transfer, by increasing the concentration of the nanofluid the thermal conductivity of the nanofluid was increased, which increased the heat transfer coefficient of fluid, resulting in the effectiveness of the heat exchanger. So, by increasing the particle volumetric concentrations, TAC also increased almost linearly. In fact, an enhancement of the concentration of the nanofluid leads to an increase in the pressure drop, which, as shown in Fig. 6, led to an increase in TAC.

1. Objective Functions for Five Optimum Points ($\dot{m}_c$=1 kg/s, $\dot{m}_h$=3 kg/s)

The optimum Pareto front is shown in Fig. 7 with different nano-

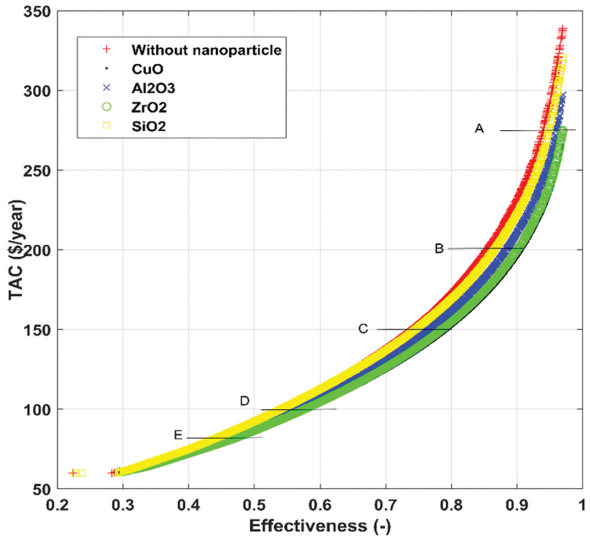


Fig. 7. Optimal Pareto fronts in the case of without nanoparticles and different nanoparticle additive and for cooling fluid mass flow rate of 1 kg/s.

fluids (copper oxide, zirconium oxide, aluminum oxide, and silicon oxide) and base fluid at a cold-side flow rate of 1 kg/s along with five optimal points. The results indicate a contradiction between the two objective functions (effectiveness and TAC). It is seen in Fig. 7 that, as an example for copper oxide nanofluid, the highest effectiveness occurred at point A (0.9698), while this value was calcu-

Table 6. Design parameters and objective functions for five optimum points A-E in Fig. 2(a) in the case of without nanoparticles

	A	B	C	D	E
Corrugation wavelength (mm)	3.1	3.7	3.7	5.1	6.1
Corrugation amplitude (mm)	1	1	2.9	4.2	4.6
Plate width (m)	0.628	0.419	0.555	0.418	0.262
Plate length (m)	0.303	0.3	0.3	0.3	0.3
Corrugation angle (degree)	65	65	65	65	65
Number of plate (-)	74	71	15	10	12
Effectiveness (-)	0.9330	0.8559	0.7332	0.5398	0.4326
TAC ($/year)	263.1	200	150	100	80

Table 7. Design parameters and objective functions for five optimum points A-E in Fig. 7 in the case of CuO

	A	B	C	D	E
Corrugation wavelength (mm)	3.1	3	3.8	5.1	6.4
Corrugation amplitude (mm)	1	1.6	2.8	3.7	4.1
Plate width (m)	0.702	0.655	0.675	0.271	0.246
Plate length (m)	0.318	0.3	0.3	0.3	0.3
Corrugation angle (degree)	65	65	65	65	65
Number of plate (-)	56	25	12	15	13
PVC (-)	0.04	0.04	0.04	0.04	0.04
Effectiveness (-)	0.9698	0.9109	0.7949	0.5889	0.4670
TAC ($/year)	263.1	200	150	100	80

Table 8. Design parameters and objective functions for five optimum points A-E in Fig. 7 in the case of ZrO_2

	A	B	C	D	E
Corrugation wavelength (mm)	3	3	3.6	5	6.9
Corrugation amplitude (mm)	1.1	1.9	4.6	4.4	3.1
Plate width (m)	0.487	0.283	0.364	0.208	0.327
Plate length (m)	0.303	0.3	0.303	0.3	0.302
Corrugation angle (degree)	65	65	65	65	65
Number of plate (-)	80	51	13	16	13
PVC (-)	0.04	0.04	0.04	0.04	0.04
Effectiveness (-)	0.9623	0.8989	0.7836	0.5746	0.4587
TAC ($/year)	263.1	200	150	100	80

Table 9. Design parameters and objective functions for five optimum points A-E in Fig. 7 in the case of Al_2O_3

	A	B	C	D	E
Corrugation wavelength (mm)	3.1	3.5	3.9	5	6.2
Corrugation amplitude (mm)	1	1.2	2.1	5.12	5.1
Plate width (m)	0.762	0.774	5.4	0.204	0.202
Plate length (m)	0.308	0.3	0.3	0.3	0.3
Corrugation angle (degree)	65	65	65	65	65
Number of plate (-)	54	32	19	15	13
PVC (-)	0.0394	0.0381	0.0394	0.04	0.0368
Effectiveness (-)	0.9556	0.8855	0.7639	0.5598	0.4432
TAC ($/year)	263.1	200	150	100	80

lated for zirconium oxide, aluminum oxide, silicon oxide nanofluids, and the base fluid at 0.9623, 0.9556, 0.9403, and 0.9330, respectively. TAC also maximized at point A for copper oxide (263.1 $/year). In addition, for fixed values of TAC of 200 $/yaer, the effectiveness of the case without nanoparticles (base fluid) and for copper oxide, zirconium oxide, aluminum oxide, and silicon oxide

Table 10. Design parameters and objective functions for five optimum points A-E in Fig. 7 in the case of SiO_2

	A	B	C	D	E
Corrugation wavelength (mm)	3.1	3.2	5	4.9	6.1
Corrugation amplitude (mm)	1	1	1.4	4.9	5.3
Plate width (m)	0.505	0.507	0.304	0.275	0.201
Plate length (m)	0.314	0.314	0.3	0.3	0.3
Corrugation angle (degree)	65	65	65	65	65
Number of plate (-)	77	71	57	12	14
PVC (-)	0.0394	0.0394	0.0356	0.0063	0.00063
Effectiveness (-)	0.9403	0.8628	0.7390	0.5416	0.4332
TAC ($/year)	263.1	200	150	100	80

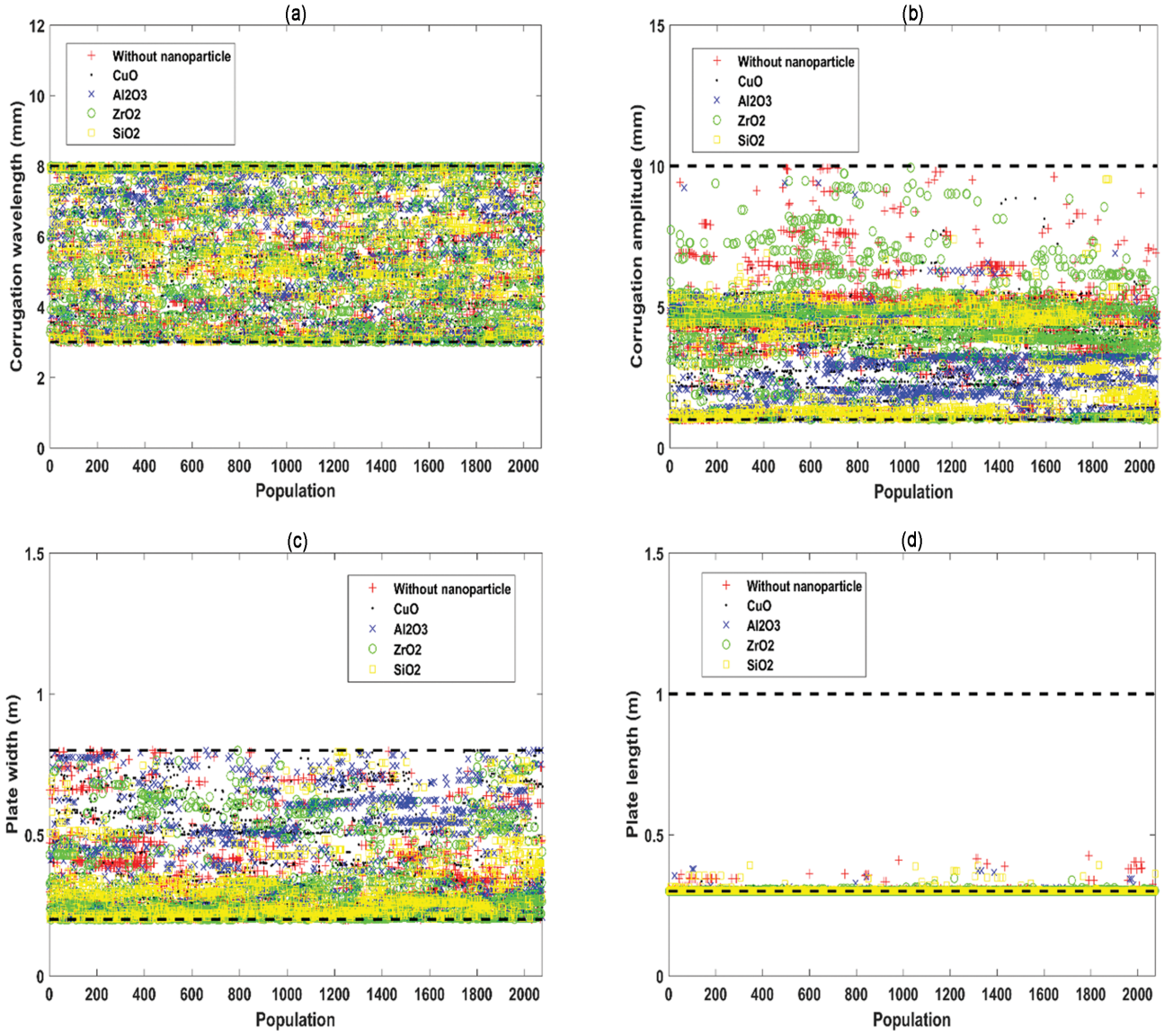


Fig. 8. Scattering of variables for the Pareto optimal front: (a) corrugation wavelength; (b) corrugation amplitude; (c) plate width; (d) plate length; (e) corrugation angle; (f) number of plates; (g) particle volumetric concentration.

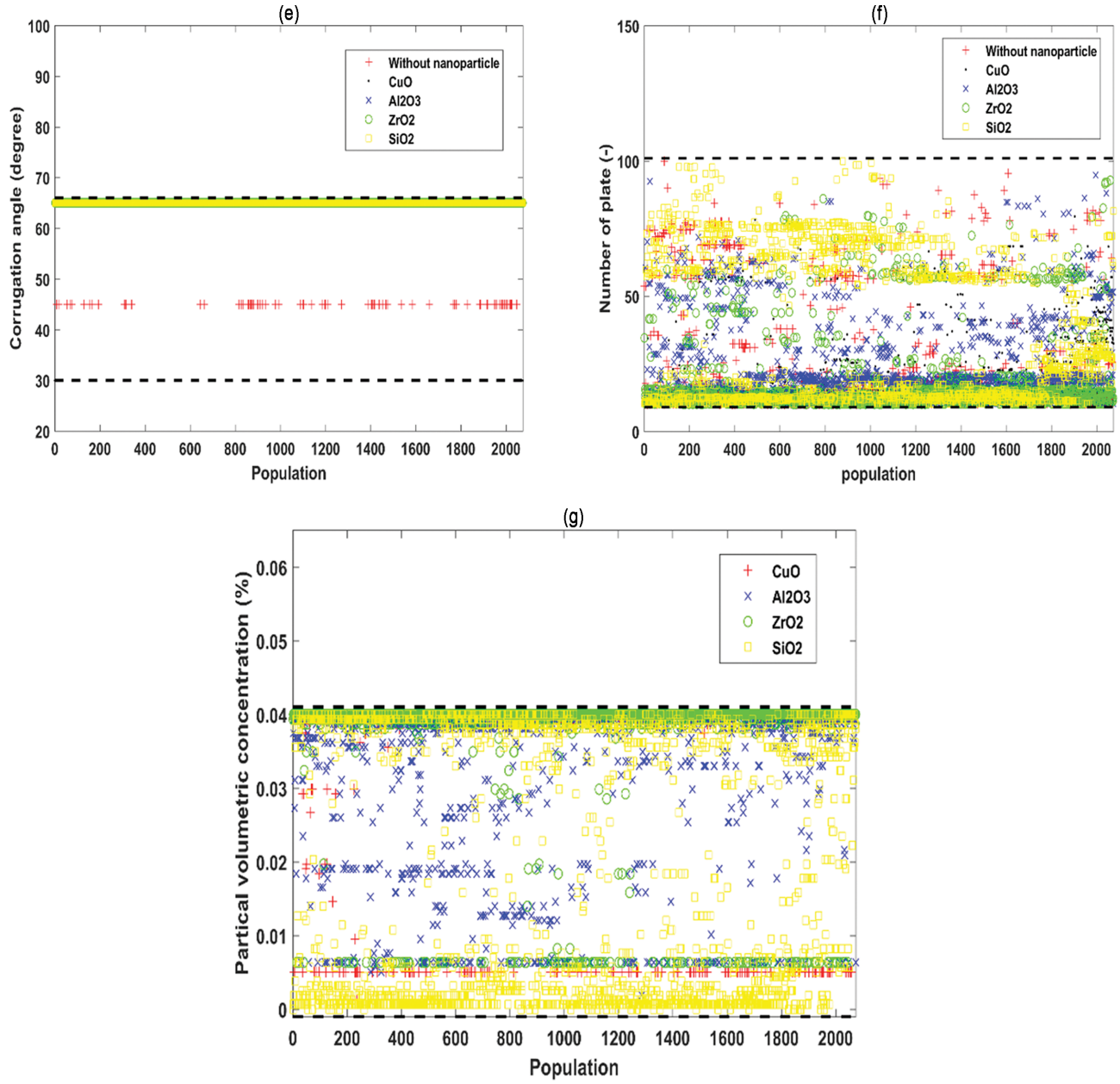


Fig. 8. Continued.

nanofluids were calculated to be 0.8559, 0.9109, 0.8989, 0.8855, and 0.8628, respectively, whereas the effectiveness growth percentages for copper oxide, zirconium oxide, aluminum oxide, and silicon oxide nanofluids were 6.42%, 5.02%, 3.45% and 0.81% versus the case in which without nanoparticles was applied, respectively.

The lowest effectiveness at point E for the case without nanoparticles and copper oxide, zirconium oxide, aluminum oxide, silicon oxide nanofluids, and base fluid were obtained at 0.4326, 0.4670, 0.4587, 0.4432, and 0.4332, respectively. The results of five optimum points are provided in Tables 6-10 for optimum distribution of optimal values of decision variables and consider functions for the states in which different or without nanoparticle were applied.

The scattering of the parameters for the optimum points on the Pareto front (Fig. 7) is illustrated in Figs. 8(a)-(f). The range of parameter changes is highlighted by dotted lines. The following points could be assumed for the optimal variables in Fig. 8:

1. The wavelength of corrugation, plate width, and particle volumetric concentration has the value dispersed in the same way over its whole acceptable domain.
2. The numerical values of the number of plates, amplitude of corrugation, and plate length are dispersed in their minimum permissible domain.
3. The numerical values of the corrugation angle are at their highest level.

Because the optimal values of wavelength of corrugation, plate width, and particle volume concentration of the nanoparticles were

Table 11. Final optimum objective functions for the several price of nanoparticles

	Price	SiO_2	Al_2O_3	ZrO_2	CuO
Effectiveness (-)	250 ($/kg)	0.6493	0.6530	0.6599	0.6599
	300 ($/kg)	0.6498	0.6559	0.6576	0.6631
	400 ($/kg)	0.6501	0.6545	0.6578	0.6628
TAC ($/year)	250 ($/kg)	122.6	118.7	115.8	113.4
	300 ($/kg)	123.7	120.4	116.3	115.2
	400 ($/kg)	124.2	122.1	118.3	117.1

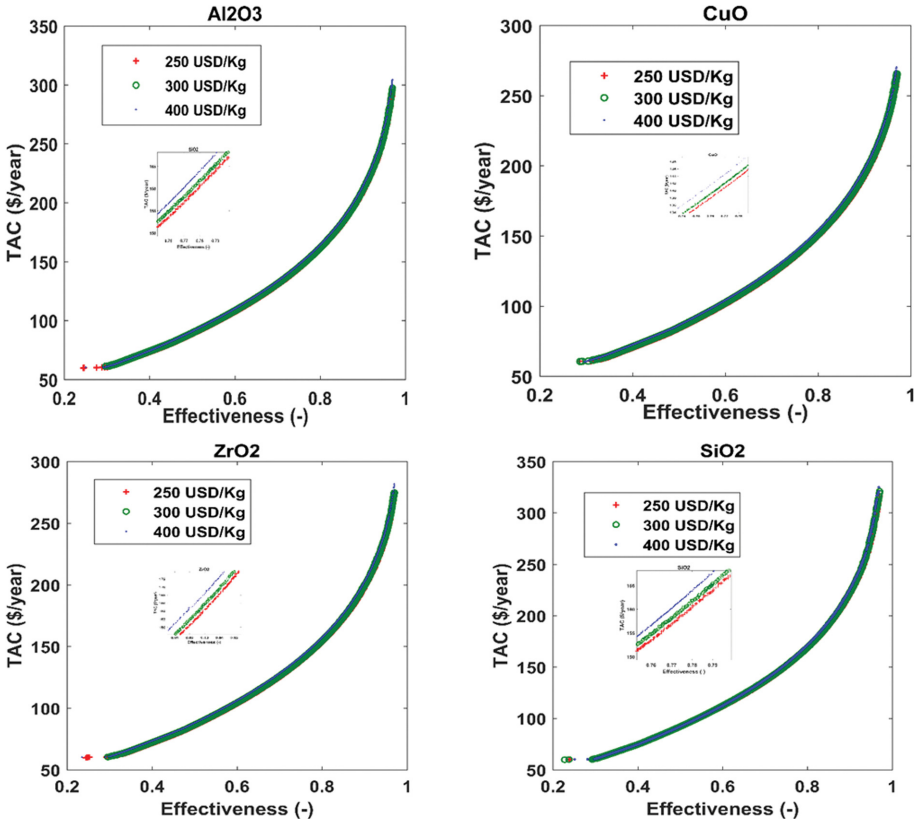


Fig. 9. Optimal Pareto fronts in the case of several nanoparticle prices for different nanofluid.

distributed almost equally across all of their permitted domains, it can be forecasted that these three variables had a significant effect on the contradiction between effectiveness and TAC. By examining the corrugation angle, it can be concluded that because it had the highest value, it had little effect on the contradiction between the effectiveness and TAC. Additionally, corrugation amplitude, plate length, and the number of plates had a sensible influence on the contradiction among the two objective functions.

2. Sensitivity Analysis on Different Prices of Nanoparticles

To have a proper insight into the influence of nanoparticle prices on the objective functions (effectiveness and TAC), optimization was made at different prices of nanoparticles, including 250, 300, and 400 USD/kg. Subsequently, the percentage of improvement in TAC for different nanofluids at the final optimum point was calculated, whose results are presented in Table 11. In addition, the optimum Pareto front diagrams for copper oxide, zirconium oxide, aluminum oxide, and silicon oxide nanofluids at different prices are shown in Fig. 9. As can be seen from the results of Table 11, at the final optimum point, a decrease or increase in the price of nanoparticles does not significantly affect the effectiveness of the heat exchanger, it changes TAC. For example, if the price of nanoparticles is considered to increase to 300 USD/year from 250 USD/year, the increasing rates of TAC for copper oxide, zirconium oxide, aluminum oxide, and silicon oxide nanoparticles will be 1.59%, 0.43%, 1.43%, and 0.9%, respectively.

CONCLUSIONS

The effects of different nanoparticles on the thermo-economic optimization of GPHE were explored at various cold-side mass flow rates of 1, 1.5, and 2 kg/s. Different nanofluids, including CuO, ZrO_2, Al_2O_3, and SiO_2, were used in this work. For this goal, the heat exchanger was optimized by the NSGA-II algorithm, and the results were compared with each other and with the case without

nanoparticles. For this purpose, effectiveness and TAC were considered as two objective functions and seven decision variables were selected. The following results were concluded:

- Thermoeconomic improvement was found at lower cold-side mass flow rates when nanoparticles were used in comparison to the case in which base fluid was used.
- The effectiveness increased by 2.61%, 1.76%, 1.50%, and 0.56% when CuO, ZrO_2, Al_2O_3, and SiO_2 were used, respectively, as compared with the case of base fluid, and TAC was reduced by 6.8%, 5.9%, 2.59%, respectively. But TAC increased by 0.08% when SiO_2 nanoparticles were used.
- 6.42% enhancement in the effectiveness was observed in the case of CuO shape as compared with the base fluid for the fixed value of TAC=200 $/year. The mentioned improvements were 5.02%, 3.45% and 0.81% for the cases of ZrO_2, Al_2O_3 and SiO_2.
- The price of nanoparticles is considered to increase to 300 USD/year from 250 USD/year, the increased rates of TAC for copper oxide, zirconium oxide, aluminum oxide, and silicon oxide nanoparticles will be 1.59%, 0.43%, 1.43%, and 0.9%, respectively.
- The effectiveness and TAC decreased with an increase in the corrugation wavelength while with an increase in the plate length of the heat exchanger, the effectiveness and TAC were increased.
- Because the optimal values of wavelength of corrugation, width of the plate, and particle volume concentration of the nanoparticles were distributed almost equally across all of their permitted domains, it can be forecasted that these three variables will have a significant effect on the contradiction between effectiveness and TAC.

NOMENCLATURE

A_{tot} : total heat transfer surface area [m^2]
a_f : annualized factor [-]
a : chevron corrugation amplitude [mm]
c_p : specific heat [J/kg·K]
C_{min} : minimum of C_h and C_c [W/K]
C_{max} : maximum of C_h and C_c [W/K]
C_{inv} : investment cost [$]
C_{np} : cost of nanoparticles supply [$]
C_{op} : operational cost [$/year]
D_{hyd} : hydraulic diameter [m]
f : fanning friction factor [-]
G : mass flux [$kg/m^2 \cdot s$]
h : heat transfer coefficient [W/m^2 K]
i : interest rate [-]
K : thermal conductivity [$Wm^{-1}K^{-1}$]
k_{el} : unit price of electricity [$/kWh]
L_p : plate length [m]
$\dot{m}$: mass flow rate [kg/s]
N : number of chevron plates [-]
Nu : Nusselt number [-]
NTU : number of transfer units [-]
PVC : particle volumetric concentration [-]
Pr : Prandtl number [-]
Re : Reynolds number [-]
R_f : fouling resistance [$K \cdot m^2/W$])
T : temperature [K]
U : overall heat transfer coefficient [W/m^2 K]
V_t : volumetric flow rate [m^3/s]
W : plate width [m]
y : depreciation time [year]
Z_{NP} : unit price of nanoparticles [$/kg]

Greek Symbols

μ : viscosity [$kgm^{-1}s^{-1}$]
Ø : particle volumetric concentration [-]
η_p : pump effectiveness [-]
ρ : density [kg/m^3]
ε : effectiveness [-]
Λ : chevron corrugation angle [mm]
β : corrugation angle [deg]
τ : hours of operation per year

Subscripts

bf : base fluid
c : cold side
h : hot side
m : medium
nf : nanofluid
np : nanoparticles
tot : total
w : wall

DECLARATIONS

Funding

The authors did not receive support from any organization for the submitted work.

Financial Interests

The authors have no relevant financial or non-financial interests to disclose.

Conflicts of Interest/Competing Interests

The authors have no conflicts of interest to declare that are relevant to the content of this article.

Availability of Data and Material

The data will be made available on request

Code Availability

The Code will be made available on request

Authors' Contributions

H. Hajabdollahi suggested the idea and stated the theory; M. Ataeizadeh performed optimization; M. Shafiey wrote the manuscript with support from H. Hajabdollahi; all authors discussed the results and contributed to the final manuscript; Both authors read and approved the final manuscript.

Ethical Approval

This article does not contain any studies with human participants or animals performed by any of the authors.

REFERENCES

1. R. K. Shah and D. P. Sekulic, *Fundamentals of heat exchanger design*, John Wiley & Sons (2003).
2. W. M. Kays and A. L. London, *Compact heat exchangers*, McGraw-Hill Book Company, Inc., New York, N. Y (1958).
3. M. Imran, N. A. Pambudi and M. Farooq, *Case Stud. Therm. Eng.*, **10**, 570 (2017).
4. C. Gulenoglu, F. Akturk, S. Aradag, N. S Uzol and S. Kakac, *Int. J. Therm. Sci.*, **75**, 249 (2014).
5. A. Yildiz and M. A. Ersöz, *Renew. Sustain. Energy Rev.*, **42**, 240 (2015).
6. H. Shokouhmand and M. Hasanpour, *Case Stud. Therm. Eng.*, **18**, 100570 (2020).
7. H. I. Mohammed, D. Giddings, G. S. Walker, P. Talebizadehsardari and J. M. Mahdi, *Int. Commun. Heat Mass Transfer*, **117**, 104773 (2020).
8. Y. Ju, T. Zhu, R. Mashayekhi, H. I. Mohammed, A. Khan, P. Talebizadehsardari and W. Yaïci, *J. Nanomater.*, **11**(6), 1570 (2021).
9. A. K. Gholap and J. A. Khan, *Appl. Energy*, **84**(12), 1226 (2007).
10. H. I. Mohammed, D. Giddings and G. S. Walker, *Int. J. Heat Mass Transfer*, **125**, 218 (2018).
11. H. I. Mohammed and D. Giddings, *Int. J. Therm. Sci.*, **146**, 106099 (2019).
12. F. Hajabdollahi, Z. Hajabdollahi and H. Hajabdollahi, *Heat Transfer Res.*, **44**(8) (2013).
13. H. I. Mohammed, D. Giddings and G. S. Walker, *Int. J. Heat Mass Transfer*, **130**, 710 (2019).
14. R. S. Vajjha and D. K. Das, *Int. J. Heat Mass Transfer*, **52**(21-22), 4675 (2009).
15. R. S. Vajjha and D. K. Das, *Int. J. Heat Mass Transfer*, **55**(15-16), 4063 (2012).
16. K. V. Sharma, P. K. Sarm, W. H. Azmi, R. Mamat and K. Kadirgama, *Int. J. Microscale and Nanoscale Therm. Fluid Transp. Phenom*, **3**(4), 1 (2012).
17. R. Lotfi, Y. Saboohi and A. M. Rashidi, *Int. Commun. Heat Mass Transfer*, **37**(1), 74 (2010).
18. T. Maré, S. Halelfadl, O. Sow, P. Estellé, S. Duret and F. Bazantay, *Exp. Therm Fluid Sci.*, **35**(8), 1535 (2011).
19. Z. Guo, *J. Enhanced Heat Transfer*, **27**(1) (2020).
20. A. K. Tiwari, P. Ghosh and J. Sarkar, *Exp. Therm Fluid Sci.*, **49**, 141 (2013).
21. M. N. Pantzali, A. A. Mouza and S. V. Paras, *Chem. Eng. Sci.*, **64**(14), 3290 (2009).
22. V. Kumar, A. K. Tiwari and S. K. Ghosh, *Energy Convers. Manage.*, **118**, 142 (2016).
23. Z. Taghizadeh-Tabari, S. Z. Heris, M. Moradi and M. Kahani, *Renew. Sustain. Energy Rev.*, **58**, 1318 (2016).
24. D. Huang, Z. Wu and B. Sunden, *Int. J. Heat Mass Transfer*, **89**, 620 (2015).
25. H. Hajabdollahi, M. Ataeizadeh, B. Masoumpour and M. S. Dehaj, *Heat Transfer Res.*, **52**(3) (2021).
26. H. Hajabdollahi, B. Masoumpour and M. Ataeizadeh, *Heat Transfer*, **50**(1), 56 (2021).
27. M. S. Dehaj and H. Hajabdollahi, *Int. J. Env. Sci. Technol.*, **19**(3), 1407 (2022).
28. S. Kakac, H. Liu and A. Pramuanjaroenkij, *HEs: selection, rating, and thermal design*, CRC press (2012).
29. J. Branke, J. Branke, K. Deb, K. Miettinen and R. Slowiński, *Lect. Notes Comput. Sci.*, 5252 (2008).
30. H. Hajabdollahi, *Appl. Therm. Eng.*, **82**, 152 (2015).